

A comparative study on the switching kinetics of W/VO₂ powders and VO₂ coatings and their implications for thermochromic glazing

Peer-reviewed author version

CALVI, Lavinia; Leufkens, Luc; Yeung, Cindy P.K.; Habets, Roberto; MANN, Daniel; ELEN, Ken; HARDY, An; VAN BAEL, Marlies & BUSKENS, Pascal (2021) A comparative study on the switching kinetics of W/VO₂ powders and VO₂ coatings and their implications for thermochromic glazing. In: Solar Energy Materials and Solar Cells, 224 (Art N° 110977).

DOI: 10.1016/j.solmat.2021.110977

Handle: <http://hdl.handle.net/1942/33331>

A comparative study on the switching kinetics of W/VO₂ powders and VO₂ coatings and their implications for thermochromic glazing

Lavinia Calvi,^{a,b} Luc Leufkens,^{c,d} Cindy P. K. Yeung,^{c,d} Roberto Habets,^{c,d} Daniel Mann,^{c,d} Ken Elen,^{a,b} An Hardy,^{a,b} Marlies K. Van Bael,^{a,b} Pascal Buskens^{*,a,c,d,e}

^aHasselt University, Institute for Materials Research (IMO), DESIne group, Martelarenlaan 42, 3500 Hasselt, Belgium.

^bIMEC vzw, IMOMEC Associated Laboratory, Wetenschapspark 1, B-3590 Diepenbeek, Belgium

^cThe Netherlands Organisation for Applied Scientific Research (TNO), High Tech Campus 25, 5656AE Eindhoven, The Netherlands

^dBrightlands Materials Center, Urmonderbaan 22, 6167RD Geleen, The Netherlands

^eZuyd University of Applied Sciences, Nieuw Eyckholt 300, 6400AN Heerlen, The Netherlands

Abstract

Monoclinic VO₂ (M) displays thermochromic properties based on its reversible metal-insulator transition. We studied the kinetics of the underlying structural phase transition (SPT) from monoclinic VO₂ (M) to rutile VO₂ (R) and *vice versa* both in powders and coatings, using isoconversional kinetic analysis based on datasets obtained through differential scanning calorimetry and UV-vis-NIR spectrophotometry. For VO₂ powders, prepared via solution-phase reduction of V₂O₅ with oxalic acid and subsequent thermal anneal, we show that the activation energy $|E_a|$ of the SPT is temperature dependent, and decreases with increasing difference between the material's temperature and the critical switching temperature T_0 . $|E_a|$ for both VO₂ (M) to VO₂ (R) and VO₂ (R) to VO₂ (M) is similar, and ranges between 138 and 563 kJ·mol⁻¹, depending on the temperature of the material. This indicates that similar defects play a key role in both SPTs. Upon doping with tungsten, T_0 was lowered from 66.93 °C (0 at. % W) to -28.38 °C (3.5 at. % W). $|E_a|$, however, remained in the same range. Nonetheless, at W concentrations above 2 at. % a significant asymmetry was observed with higher $|E_a|$ for the switch from VO₂ (R) to VO₂ (M). The SPT of VO₂ (M) in coatings proceeded 4 times slower. This may result from the immobilization of the VO₂ domains on the substrate surface and within the coating network, making the SPT more difficult to progress. The findings of this study have important implications for the application of VO₂ (M) in energy efficient thermochromic glazing.

1. Introduction

The V-O phase diagram is complex and comprises a great variety of compounds and crystal phases. Because of its thermochromic properties monoclinic vanadium dioxide VO₂ (M) is one of the species of interest.[1,2] At the critical switching temperature (T_0), which is approximately 68 °C for undoped VO₂ (M),[3] this material undergoes a structural phase transition (SPT) from monoclinic to tetragonal rutile structured VO₂ (R) (Fig. 1). This SPT is reversible and can be considered as a continuous process with a succession of intermediate structures between VO₂ (M) and VO₂ (R).[4] Fig. 1 graphically represents the crystal structures of VO₂ (M) and VO₂ (R). During the transition from VO₂ (M) to VO₂ (R) the symmetry increases as vanadium atoms become equidistant (Wyckoff positions), and are each surrounded by oxygen atoms in an edge-sharing octahedron.[1] During the SPT the distance between the V atoms changes. V-V1a undergoes elongation while V-V1b shortens (Fig. 1), the zigzag chain undergoes a twist and becomes a linear chain ($\delta=0^\circ$),[4] and the unit cell volume halves in size.[5]

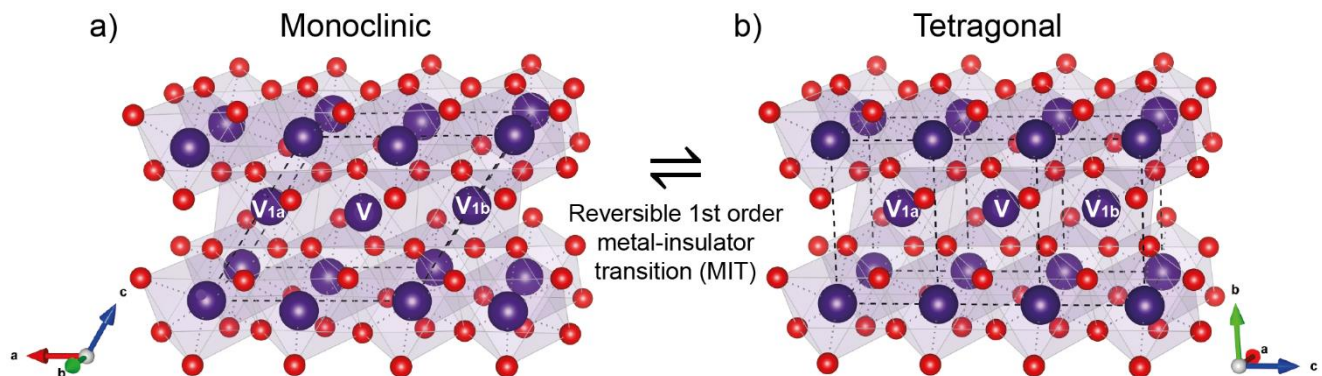


Fig. 1. The monoclinic and tetragonal rutile crystal structure of VO₂, where purple is V and red is O, drawn with VESTA 3 software.[35]

Since $\text{VO}_2(\text{M})$ is a semiconductor and $\text{VO}_2(\text{R})$ is an electrical conductor, the SPT is accompanied by a first order metal-insulator transition (MIT).[1,5,6] During the transition from $\text{VO}_2(\text{R})$ to $\text{VO}_2(\text{M})$, from Goodenough theories the distortion to the zig-zag structure causes a shift in the π^* band above the Fermi energy, which leads to an increase in the bandgap from 0.7 eV (metallic, Fig. 2b) to 2.5 eV (semiconducting, Fig. 2a).[5,7] The SPT and accompanying MIT are of interest for applications in coatings or particulate materials for energy efficient glazing:[8–11] as a consequence of its semiconducting properties, $\text{VO}_2(\text{M})$ displays a high transmission for solar infrared (IR) radiation at low temperatures, whilst the metallic tetragonal phase blocks IR light at elevated temperatures.[12–16] Recent studies show that smart windows comprising such thermochromic coatings may lead to significant reduction in energy consumption for heating and cooling of buildings in intermediate climates.[8,17,18]

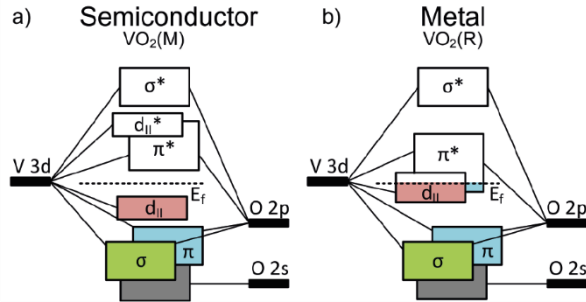


Fig. 2. Band structure of the semiconductor $\text{VO}_2(\text{M})$ and the metallic $\text{VO}_2(\text{R})$; image based on Ramanathan (2010).[7]

For most applications, such as smart windows,[19] sensors,[19] electronic devices,[19] actuators,[19] power meters or thermometers,[19] optical and holographic devices,[19] ionic gratings,[20] improved computational approaches,[20] and new ultrafast microscopy techniques,[20] T_0 needs to be adjusted. For instance in case of thermochromic windows, T_0 needs to be lowered from 68 °C to 15-25 °C for optimum energy savings. [8,18] Furthermore, understanding and tuning kinetics of the switch are important, to ensure a quick response of the material to the changing environmental conditions.

T_0 of $\text{VO}_2(\text{M})$ can be influenced by intrinsic point defects, dopants and strain.[21] Oxygen vacancies and cation non-stoichiometry (intrinsic point defects) lower the valence state of V, narrowing the band gap of the $\text{VO}_2(\text{M})$ phase.[21] The oxygen vacancies deform the crystal structure and induce polarization charges, which results in a decrease in T_0 . [21,22] Introduction of other element(s) such as W, Mg and Mo[6,23] into $\text{VO}_2(\text{M})$ is also used to modify T_0 through the distortion of the structure, which assists in the phase transition.[21]

In previous research on the thermokinetic behaviour of $\text{VO}_2(\text{M})$, Blagojević *et al.*[24] applied Flynn-Wall-Ozawa and Kissinger-Akahira-Sunose isoconversional methods to study the switching kinetics of undoped VO_2 nanoribbons and nanosheets (shortest dimension 10-20 nm and 20-30 nm, respectively) prepared via hydrothermal synthesis. They concluded that the kinetics of the SPT depend on the applied heating rate, and that the kinetic behaviour is complex as the switch consists of at least two single-step processes, independent from the dimensionality of the samples. Furthermore, they demonstrated that the activation energy is dependent on the degree of conversion of $\text{VO}_2(\text{M})$ to $\text{VO}_2(\text{R})$, and therefore covers a range of values between 150-570 kJ·mol⁻¹. [24] Additionally, Zang *et al.*[25] also used isoconversional methods to investigate the kinetics of nucleation during the SPT of hydrothermally synthesized tungsten doped VO_2 . These authors report that the activation energy is dependent on the applied temperature, and that this dependence on temperature is not symmetric for the transition of $\text{VO}_2(\text{M})$ to $\text{VO}_2(\text{R})$ and *vice versa*. In general, they report higher activation barriers for the transition from $\text{VO}_2(\text{R})$ to $\text{VO}_2(\text{M})$ and suggest that different defects are underlying both transitions. Zang *et al.* claimed that doping decreased the activation energy barrier because of an increase in effective nucleation sites.[25] However, it should be noted that their investigated powders appear to be not completely pure as demonstrated by the asymmetric and multiple DSC peaks observed for the undoped $\text{VO}_2(\text{M})$ sample.

For application purposes thermochromic $\text{VO}_2(\text{M})$ is mainly used as a coating on glass. The switching kinetics of thermochromic VO_2 coatings applied to float glass, however, have not yet been studied. Therefore, it is important to study the switching kinetics of VO_2 coatings, and compare these to the switching kinetics of particulate material prepared from the same chemical precursors in a similar chemical process.

In the current article, we investigate the kinetics of the phase transition of $\text{VO}_2(\text{M})$ in powders and coatings originating from the same chemical precursors, *i.e.* V_2O_5 and oxalic acid, and obtained after a similar thermal anneal process. The kinetics of the SPT for VO_2 powders with different concentrations of W as dopant are studied in detail, and compared to switching kinetics of coatings comprising undoped VO_2 which are applied to SiO_2 -coated float glass substrates. Furthermore, the switching kinetics of the coatings are studied as function of the coating thickness.

Finally, we discuss the impact of the obtained results on practical applications related to thermochromic energy efficient glazing (smart windows).

2. Experimental

2.1. Preparation of vanadyl oxalate solution

The vanadyl oxalate solution is prepared at 80 °C by adding vanadium(V) oxide (V_2O_5 , 33.0 g, 0.182 mol; 99.6 %, Sigma-Aldrich) to a slurry of oxalic acid ($\text{C}_2\text{H}_2\text{O}_4$, 70.2 g, 0.780 mol; 98 %, Sigma-Aldrich) in Milli-Q water (18.0 g). Subsequently, the mixture is stirred for 1 h, after which 2-propanol (150.0 g; 99.8 %, Sigma-Aldrich) is added and the resulting solution is cooled to room temperature. After 1 h stirring at room temperature, the reaction is further diluted with 2-propanol to obtain a VO_2 concentration of 0.20 or 0.40 $\text{mol}\cdot\text{kg}^{-1}$.

2.2. Preparation of silica sol

For the preparation of a silica sol, Milli-Q water (135.0 g, 7.5 mol) and acetic acid (CH_3COOH , 4.5 g, 0.075 mol; 99.9 %, Alfa Aesar) were added to a stirred solution of tetraethoxysilane ($\text{Si}(\text{OCH}_2\text{CH}_3)_4$, 156.3 g, 0.75 mol; 98 %, Acros Organics) in 2-propanol (347.3 g). After 24 h stirring at room temperature, nitric acid (1.50 g; 65 %, Fisher Chemicals) was added, and the silica sol was further diluted with 2-propanol to a SiO_2 concentration of 0.20 or 0.40 $\text{mol}\cdot\text{kg}^{-1}$.

2.3. Preparation of tungsten solution

The tungsten solution was prepared by dissolving tungsten hexachloride (WCl_6 , 99.9+ %, Acros Organics) in 2-propanol to obtain a W^{6+} concentration of 0.052 $\text{mol}\cdot\text{kg}^{-1}$.

2.4. Fabrication of thermochromic coatings

Pilkington Optiwhite[™] glass of 4 mm thickness and cut to a size of 10 x 10 cm^2 was used as substrate for application of coatings. The glass plate was placed into an ultrasonic bath filled with a mixture of ammonia (310 g, 30 wt. % in water), hydrogen peroxide (186 g, 50 wt. % in water) and demineralized water (9000 g, 18.2 $\text{m}\Omega\cdot\text{cm}$) at 60 °C. Glass plates were ultrasonicated for 4 h, then left in the bath for another 16 h. The glass plates were subsequently removed from the bath, rinsed with demineralized water and left to dry at ambient conditions. Glass substrates which did not display a homogeneous wetting of water with a contact angle below 10 ° were rejected.

Firstly, a silica barrier coating was applied on both sides of the cleaned glass substrates using dip coating, to prevent ion migration from the glass into the coating (SI1.1). For this purpose, silica sol with a SiO_2 concentration of 0.20 $\text{mol}\cdot\text{kg}^{-1}$ was used. The substrates were submerged into the silica sol and subsequently retracted at a withdrawal speed of 2.0 $\text{mm}\cdot\text{s}^{-1}$. All coating experiments were performed at a relative humidity below 35 % and a temperature between 19 and 25 °C. After application of the coating and drying under ambient conditions, the coated glass substrates were annealed in a muffle furnace (Nabertherm L5/13/B180) at a temperature of 450 °C for 1 h under air. After cooling, the annealed barrier-coated glass substrates were rinsed with demineralized water and dried under ambient conditions. Then, one side of the barrier coated glass substrate was masked using d-c-fix[®] self-adhesive film. Subsequently, the thermochromic coating was applied to the non-covered side using dip coating. The applied liquid coating formulation consisted of a mixture of vanadyl oxalate solution and silica sol at a molar ratio of SiO_2 to VO_2 of 1:2.2 (using the silica sol of a concentration of 0.20 for the 46 nm and 0.40 $\text{mol}\cdot\text{kg}^{-1}$ for the 68 and 140 nm coating). The silica sol was added as a film forming binder material. The obtained xerogel coating was applied to the glass substrates at withdrawal speeds in the range of 1.0-4.0 $\text{mm}\cdot\text{s}^{-1}$. After drying for 5 min under ambient conditions, the adhesive film was removed. The non-coated side was then placed onto a 6 inch silicon wafer, and annealed in a Jipelec[™] Jetfirst PV Rapid Thermal Processor, with the coated side facing the IR radiators. The coated glass plates were first heated to 270 °C under air for 480 s, and subsequently under N_2 (HiQ 6.0, Linde gas) at 450 °C for 30 s.

Coating thicknesses were measured using a Bruker Dektak XT-S surface profiler. For further analysis, coating material was scraped off the glass plates using a razorblade. This material was then used for scanning transmission electron microscopy – energy dispersive X-ray (STEM-EDX) analyses using a probe-corrected JEOL ARM 200F operated at 200 kV, equipped with a 100 mm^2 SDD EDS detector. The method used was High Angle Annular Dark Field (HAADF) STEM, and EDX, spot 3 C.

2.5. Fabrication of thermochromic powders

For obtaining undoped VO_2 powder, the vanadyl oxalate solution is applied. For obtaining W-doped VO_2 powders, tungsten solution is added to the vanadyl oxalate solution to achieve a doping concentration of W of 1.0, 1.5, 2.0,

2.5, 3.0 and 3.5 at. %. The resulting mixture is then stirred for 16 h at room temperature. The solvent is subsequently removed using a rotary evaporator. The dried powder is then annealed in a conventional tube furnace (Nabertherm R170/1000/12) equipped with a quartz tube. Firstly, the powder is heated under air at 270 °C for 1 h. Then, in a second anneal step the powder is heated at 1000 °C for 1 h under N₂ (purity grade 5.0). X-ray diffraction (XRD) measurements to determine the composition of the powder samples were carried out on a Bruker D8 Advance.

2.6. Procedure & data collection for the kinetics study

Differential Scanning Calorimetry (DSC) was carried out on a Discovery DSC (TA Instruments). The undoped and W-doped VO₂ powder samples (20 mg) were placed in pans (TA instruments, Tzero aluminium pan). All samples were subjected to the following four heating and cooling rates: 5, 10, 15, 20 °C·min⁻¹. As sample mass for the DSC analyses we selected 20 mg. At lower masses (5, 10 and 15 mg), the relative weighing error causes substantial deviations in the obtained results. At higher masses (30 and 40 mg), the relatively high thermal mass causes a delay and distortion in time of the heat flow signal due to heat storage within the sample, leading to an undesired broadening of the DSC signal over a broad temperature range. For further details, see SI2.

The collected data were analysed and processed in accordance with the isoconversional method, which is discussed in the following section. Using the TA instruments TRIOS software v5.0, the running integral of the DSC peak is processed to obtain a conversion-time profile. The first derivative of the conversion time plot represents the conversion rate. At 50 % conversion ($\alpha = 0.50$) the rate is obtained from this curve. Additionally, the corresponding temperature at 50 % conversion is extracted from the running integral. Then, both values are applied to produce the Friedman plot (see results and discussion). The first derivative of the Friedman plot equals the activation energy. The measurements on the coatings were carried out using a Perkin Elmer Lambda 750 UV-vis-NIR spectrometer equipped with a temperature controlled module manufactured by OMT Solutions B.V. for measuring transmission at temperatures between 0 °C and 120 °C (SI1.2). For determining the transmission in the visible and the solar modulation, the transmission was measured between 250-2400 nm at 20 °C and 120 °C after 30 min equilibration. To determine the rate of the SPT of VO₂ coatings, the coated samples were heated and cooled at 1.5 °C·min⁻¹ whilst measuring the transmission at the wavelength of 1600 nm. This allows the SPT to be monitored as a function of temperature and time. The transmission as a function of temperature is converted to a conversion-time profile in analogy to the DSC method for powders reported above, and using Lambert-Beer's Law. The conversion is extracted by setting the transmission value above 80 °C as $\alpha = 1$ and the starting transmission (around 20 °C) as $\alpha = 0$. At a conversion of 0.50 the gradient (rate of conversion) is extracted for the different coating thicknesses.

3. Results and Discussion

3.1. Phase transition kinetics theory

During the phase transition of VO₂ (M) to VO₂ (R) small nuclei of the second phase start to form within the initial phase, which is referred to as nucleation. As the nuclei grow and aggregate the new phase grows to the point of homogeneity.[26,27] The transition from monoclinic VO₂ (M) to tetragonal VO₂ (R) occurs only after the crystals are heated to a temperature above T_0 , because the nuclei of the VO₂ (R) encounter an energy barrier for this transition.[26] For the same reason, when transitioning from VO₂ (R) to VO₂ (M) the crystals need to be cooled to a temperature below T_0 . Nucleation in solids can be favoured by impurities and defects, as these facilitate diffusion and aggregation within the lattice.[25] In the VO₂ structure the vanadium atoms diffuse in the V-V direction.[21] The reaction kinetics applied to thermal analysis data can be represented by the following single-step kinetic equation, which is based on Arrhenius Law:[28]

$$\frac{d\alpha}{dt} = A \exp\left(\frac{-E}{RT}\right) f(\alpha) \quad (1)$$

Here A is a pre-exponential factor (temperature independent), E is the activation energy, R is the gas constant, T is temperature and $f(\alpha)$ is the reaction model. Applying the isoconversional principle that reaction rate is dependent only on temperature when the extent of conversion (α) from one crystal structure to the other is constant leads to the following relationship for the activation energy E_α :[28]

$$E_\alpha = -R \left(\frac{d \ln(d\alpha/dt)}{dT^{-1}} \right)_\alpha \quad (2)$$

Rearranging equation 1 leads to the foundation of the Friedman differential isoconversional method:[28,29]

$$-R \ln \left(\frac{d\alpha}{dt} \right)_{\alpha,i} = -R \ln(A_\alpha f(\alpha)) + \frac{E_\alpha}{T_{\alpha,i}} \quad (3)$$

Where i indicates the different heating rates. Plotting a graph of $-R \ln(d\alpha/dt)$ versus T^{-1} leads to the Friedman plot, in which the activation energy is the gradient (first derivative). Applying this model to nucleation, the activation barrier will correspond to the free energy barrier for the new nucleus forming (ΔG^*). The energy barrier for forming a new nucleus passes through a peak, occurring at a critical radius. Once above this radius the nucleus would grow spontaneously.[26] Assuming the formed nucleus is spherical, ΔG^* can be defined in the following way for homogeneous nucleation[26]:

$$\Delta G^* = \frac{16\pi\sigma^3 T_0^2}{3(\Delta H)^2 (\Delta T)^2} = \frac{A}{(\Delta T)^2} \quad (4)$$

Where T_0 is the critical temperature, ΔH is phase transition enthalpy, σ is the surface energy of the nucleus and A is a constant. ΔT is the difference between the temperature of the material and the critical switching temperature T_0 , and is defined as $\Delta T = T - T_0$ for heating and $\Delta T = T_0 - T$ for cooling. T_0 is the temperature at which the switch starts and where it is infinitely slow. For consistency throughout the data the value of T_0 is taken at 2 % conversion and referred to as $T_{\alpha=0.02}$. Nucleation rate has a complicated dependence on temperature, since ΔG^* depends on ΔT . Therefore, the Friedman plot results in a non-linear relationship which is in contrast with Arrhenius plots for conventional chemical reactions.[26]

Derivation of equation 3 and then substituting this into equation 2 gives the following two equations, one for heating and the other for cooling:

$$E_h = A \left(\frac{1}{(\Delta T)^2} + \frac{2T}{(\Delta T)^3} \right) \text{ or } E_c = A \left(\frac{1}{(\Delta T)^2} - \frac{2T}{(\Delta T)^3} \right) \quad (5)$$

In the following study DSC has been used for the characterization of the VO₂ powders. The extent of conversion equals the fractional enthalpy of the DSC peak. Therefore, the nucleation rate is expressed in the following manner:[29]

$$\frac{d\alpha}{dt} = \frac{dH}{A_T dt} \quad (6)$$

Where H is enthalpy of the phase transition, A_T is the area under the entire thermogram, which is the enthalpy of the entire phase transition.

The single-step equation is only applicable to the specific α which occurs in the temperature range of ΔT , therefore the kinetics of the entire process is a combination of many single-step kinetic equations.[28] This also means that E_α is not constant but depends on conversion, and therefore the constant value of $\alpha = 0.50$ is used in our study.

3.2. Thermokinetic analysis of undoped and W-doped VO₂ powders

We analysed the composition and purity of undoped and W-doped VO₂ powders, prepared according to the procedure outlined in 2.5, using XRD and DSC. The XRD of the undoped sample represents VO₂ (M) as sole crystalline material (Fig. 3a). DSC analysis confirms the high degree of purity of the sample with an average switching enthalpy of 55.4 J·g⁻¹ (Fig. 3b, Table 1), which equals the theoretical maximum for VO₂ (M).[3,12,30,31] Furthermore, both the switch from VO₂ (M) to VO₂ (R) and VO₂ (R) to VO₂ (M) are represented by well-defined symmetric peaks which do not overlap in temperature. The SPT starts ($T_{\alpha=0.02}$) at 66.93 °C and 64.95 °C upon heating and cooling, respectively. There is no overlap in the temperature range of the heating and cooling curve which agrees with equations 4 and 5 as thermodynamically an overlap cannot occur in case of a single pure species. In the W-doped

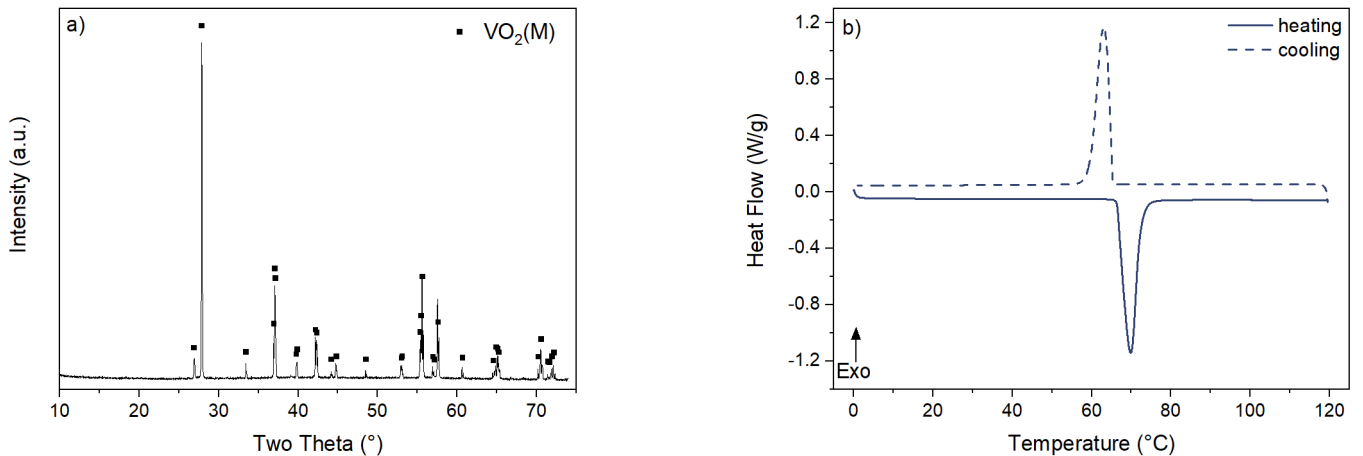


Fig. 3. a) XRD diffractogram of undoped VO₂ (M) powder, JCPDS 82-0661 and b) DSC of undoped VO₂ (M) powder obtained at a heating and cooling rate of 5 °C·min⁻¹.

samples, with a degree of doping between 1.0 at. % and 3.5 at. %, traces of V_6O_{13} were observed as crystalline impurities in the XRD (SI3). In the powders with ≥ 2 at. % W, also the presence of vanadium tungsten oxide ($V_2WO_{7.5}$) was detected. DSC analysis of the W-doped samples shows a decrease in temperature $T_{\alpha=0.02}$ with increasing dopant concentration from 66.93 °C (0 at. % W) to -28.38 °C (3.5 at. % W) for the VO_2 (M) to VO_2 (R) switch (Fig. 4, Table 1). All W-doped samples display an overlap in temperature range for the DSC peaks representing the VO_2 (M) to VO_2 (R) and VO_2 (R) to VO_2 (M) SPT. This means that upon W-doping, multiple VO_2 (M) species are formed, each probably with a different concentration of dopant. Compared to the undoped VO_2 (M), the DSC peaks broaden significantly, and multiple underlying peaks become apparent (Fig. 4). With increasing concentration of dopant, the switching enthalpy decreases, which is in agreement with reports by multiple other research groups.[12,32–34] At relevant switching temperatures for application in smart glazing, we obtained switching enthalpies of 30.3 J·g⁻¹ (2 at. % W, $T_{\alpha=0.02}$ = 18.02 °C) and 27.5 J·g⁻¹ (2.5 at. % W, $T_{\alpha=0.02}$ = 1.34 °C). Both the undoped and W-doped powders contain particulate sizes in the range of 1-10 μ m, determined by SEM analyses performed at room temperature (SI4). The VO_2 powders with a W concentration between 0-1.5 at. % W tend to consist of isometric particles with smooth edges. Compared to the undoped powder with merely particles of a size above 1 μ m, the W-doped samples display a substantial share of particles with a size below 1 μ m. The particles comprising 2.0-3.5 at. % W are anisometrically shaped and have more sharp edges. This can be explained by the composition of the sample: up to 1.5 at. % W, the sample mainly contains VO_2 (M) at room temperature, whilst for higher concentrations the material consists of a mixture of VO_2 (M) and VO_2 (R). To detect potential switching fatigue, we subjected the undoped VO_2 powder to 30 cycles in the DSC. No change in performance was observed for both SPTs (SI5) as the peak temperature and enthalpy remains unchanged throughout the 30 cycles.

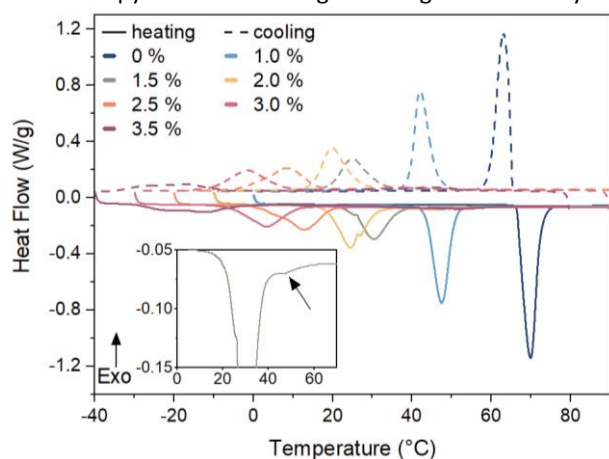


Fig. 4. DSC of undoped and W-doped VO_2 powders at a heating rate of 5 °C·min⁻¹.

Table 1. Temperature at 2 and 50 % conversion of the undoped and W-doped VO_2 powder samples at 5 °C·min⁻¹ and average enthalpy for all heating rates (5, 10, 15 and 20 °C·min⁻¹).

W concentration (atm. %)	$T_{\alpha=0.02}$ (°C)		$T_{\alpha=0.50}$ (°C)		Average enthalpy ΔH (J·g ⁻¹)	
	VO_2 (M) to VO_2 (R)	VO_2 (R) to VO_2 (M)	VO_2 (M) to VO_2 (R)	VO_2 (R) to VO_2 (M)	VO_2 (M) to VO_2 (R)	VO_2 (R) to VO_2 (M)
0	66.93	64.95	69.27	63.27	55.4 ± 0.1	55.1 ± 0.1
1.0	42.38	48.04	46.93	42.79	41.3 ± 0.1	41.5 ± 0.1
1.5	21.63	45.07	30.63	25.81	26.1 ± 0.2	25.7 ± 0.1
2.0	18.02	42.73	24.85	20.85	30.4 ± 0.2	30.2 ± 0.1
2.5	1.34	45.23	13.01	9.11	27.7 ± 0.5	27.3 ± 0.2
3.0	-6.67	47.37	3.88	-0.11	24.5 ± 0.9	24.6 ± 0.6
3.5	-28.38	52.47	-10.24	-13.56	17.1 ± 0.1	17.3 ± 0.1

For studying the kinetics of the SPT, we performed DSC analyses using heating and cooling rates of 5, 10, 15 and 20 °C·min⁻¹ (Fig. 5a, 0 at. % W). The resulting DSC profiles (Fig. 5a) were converted into conversion-time plots (Fig. 5b), from which the reaction rate at 50 % conversion was determined. Together with the T at 50 % conversion ($T_{\alpha=0.50}$), this information forms the base for the Friedman plot (Fig. 5c) of which the first derivative corresponds to the activation energy. The Friedman plot shows that the activation energy for the SPTs VO_2 (M) to VO_2 (R) and VO_2 (R)

to VO₂ (M) is temperature dependent since the relationship between $-\ln(d\alpha/dt)$ and $1000/T$ is non-linear.

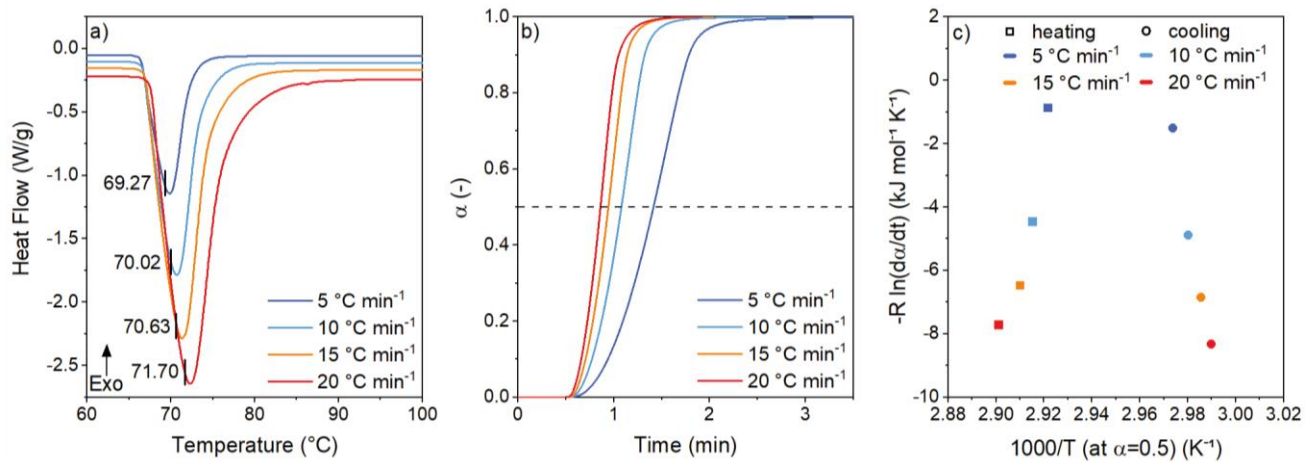


Fig. 5. a) DSC heating curves for undoped VO₂ powder at different heating rates, the indicated values correspond to the temperature at $\alpha = 0.50$, b) Conversion-time profile of VO₂ (M) to VO₂ (R) at different heating rates (running integral of DSC curve with respect to time), c) Friedman plot at $\alpha = 0.50$ for the VO₂ (M) to VO₂ (R) SPT and vice versa.

Furthermore, the Friedman plot is symmetric, indicating that both SPTs have a similar activation barrier. Additionally, for both SPTs the activation barrier rises steeply when approaching the critical switching temperature T_0 . With increasing ΔT the activation energy decreases rapidly. To determine the activation energy $|E_a|$, we determined the slope of a straight line between two consecutive data points in the Friedman plot, and attributed the corresponding $|E_a|$ to the temperature in the middle of both data points $((T_1 + T_2)/2)$. For the SPT of undoped VO₂ (M) to VO₂ (R) $|E_a|$ ranges between 138 kJ·mol⁻¹ ($T = 71.2$ °C) and 563 kJ·mol⁻¹ ($T = 69.6$ °C). For the SPT from VO₂ (R) to VO₂ (M) $|E_a|$ ranges between 353 kJ·mol⁻¹ ($T = 61.7$ °C) and 523 kJ·mol⁻¹ ($T = 62.9$ °C) (Table 2). Since the values obtained for both switches are similar, we anticipate that similar defects play an essential role in promoting both SPTs. The standard deviation on the activation energy for the SPT of undoped VO₂ powder ranges from 9 kJ·mol⁻¹ to 37 kJ·mol⁻¹ (SI6).

Table 2. Activation energy determined for the SPT of undoped and W-doped VO₂ (M) powders.

W conc. (atm. %)	VO ₂ (M) to VO ₂ (R)		VO ₂ (R) to VO ₂ (M)	
	$ E_a $ (kJ·mol ⁻¹)	T (°C)	$ E_a $ (kJ·mol ⁻¹)	T (°C)
0	563	69.6	523	62.9
	388	70.3	367	62.2
	138	71.2	353	61.7
1.0	448	47.4	463	42.4
	306	48.2	285	41.6
	160	49.1	216	40.8
1.5	not determined		692	25.5
	353	31.0	370	24.8
	267	31.7	265	24.2
2.0	1382	25.0	751	20.6
	405	25.5	442	20.0
	301	26.1	299	19.5
2.5	648	13.3	929	8.9
	434	14.0	450	8.4
	256	14.6	297	7.9
3.0	355	4.4	753	-0.4
	359	5.2	401	-0.9
	236	5.8	291	-1.4
3.5	321	-10.4	984	-14.7
	250	-9.4	2123	-15.0
	208	-8.6	350	-15.2

Upon doping with W, the activation energy remains temperature dependent. This dependency is similar to the one reported for non-doped VO₂ (M) powder. The W-doped systems are complex and do not comprise one single switching species (*vide supra*). Therefore, the activation energy determined from the Friedman plot represents merely an average activation energy for multiple simultaneously occurring switches of species with different W concentrations. We observed that the activation barrier for undoped and W-doped powders is similar since the calculated average activation energies are in the same range (Fig. 6, Table 2). Up to a W concentration of 2 at. %, the switching behaviour is symmetric. For higher W concentrations, however, we observe a significant asymmetry with higher activation energies for the SPT from VO₂ (R) to VO₂ (M). This indicates that, in line with the results obtained for the non-doped sample, similar defects play a key role in the SPT from VO₂ (M) to VO₂ (R) and *vice versa* up to a W concentration of 2 at. %. At higher concentrations, it is reasonable to assume that different defects facilitate both SPTs. This is in agreement with the results reported by Zang *et al.*[25] for hydrothermally synthesised W-doped VO₂ nanoparticles, where asymmetric behaviour with a higher barrier for the VO₂ (R) to VO₂ (M) SPT was reported.

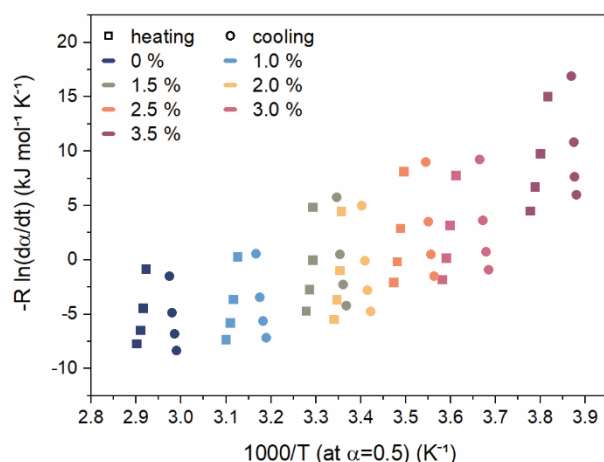


Fig. 6. Friedman plot for the W-doped powder samples at $\alpha = 0.50$ for the VO₂ (M) to VO₂ (R) SPT and *vice versa*.

3.3 Thermokinetic analysis of VO₂ coatings

Based on the similarity of the synthesis method for powders and coatings involving V(IV)-oxalate complex and the thermal anneal (see 2.5 and 2.4, respectively), it is interesting to compare the behaviour of the powders and coatings. After preparation of the coatings, we analysed the coating thickness using a Dektak profilometer. The obtained coatings had a thickness of 46 ± 8 , 68 ± 11 and 140 ± 12 nm. To study the distribution of VO₂ in the silica matrix, we performed STEM-EDX studies on the 140 nm thick coating that was scraped off from the glass substrate. The STEM-EDX images (Fig. 7) display a random distribution of VO₂ domains in the silica matrix, with a typical domain size of about 40 nm. Since these domains are substantially smaller than 100 nm, they do not cause Mie scattering, and the system yields transparent coatings (Fig. 8). Additionally, we performed DSC analysis of scraped-off coating material (Fig. 9). The ($T_{\alpha=0.02}$) for the VO₂ (M) to VO₂ (R) and VO₂ (R) to VO₂ (M) SPT was 70.30 °C and 63.13 °C, respectively. The switching enthalpy of the material, consisting of 50 vol-% silica and 50 vol-% VO₂, was 22.4 J·g⁻¹ corresponding to a degree of purity of the VO₂ material of approx. 54 %. This is substantially lower than the degree of purity obtained for VO₂ powders, which is probably caused by the fact that not all VO₂ present in the coating crystallized at the relatively low anneal temperature of 450 °C. The temperature of the second anneal step is limited by the softening temperature of float glass, which is about 470 °C. To detect potential switching fatigue, we subjected the scraped off coating material to 30 cycles in the DSC. No change in performance was observed for both SPTs as the ΔH and T_0 remained unchanged (S17).

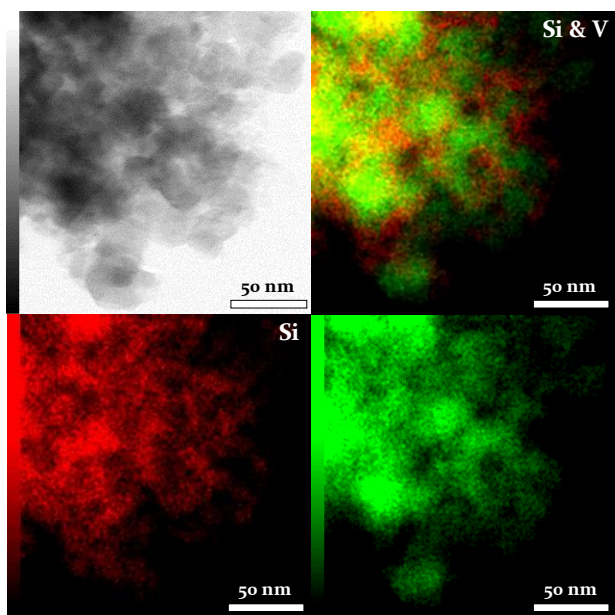


Fig. 7. STEM-EDX of scraped off coating material from the 140 nm thick coating containing VO_2 and SiO_2 in a 1:1 volume ratio (green: V & red: Si).

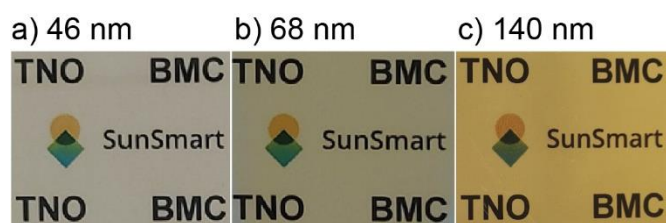


Fig. 8. VO_2 containing thermochromic coatings on SiO_2 -coated float glass with 1:1 volume ratio of VO_2 to SiO_2 , with a coating thickness of a) 46 nm, b) 68 nm and c) 140 nm.

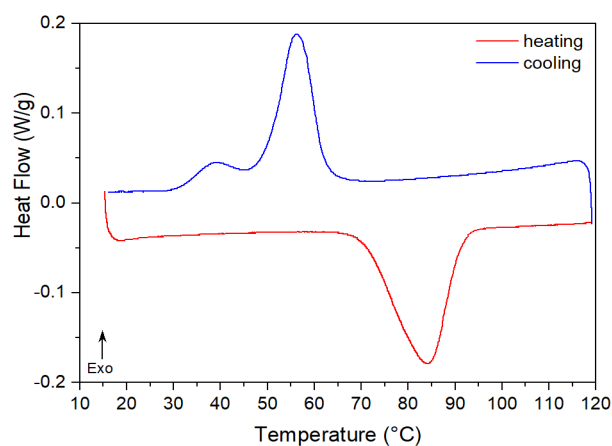


Fig. 9. DSC of scraped off coating material from the 140 nm thick coating containing VO_2 and SiO_2 in a 1:1 volume ratio, analyzed at a heating and cooling rate of $5\text{ }^\circ\text{C}\cdot\text{min}^{-1}$.

To study the thermokinetic behaviour of these coatings, we used a UV-vis-NIR spectrophotometer equipped with a temperature controlled module to perform transmission measurements between $0\text{ }^\circ\text{C}$ and $120\text{ }^\circ\text{C}$ (SI1.1). The UV-vis-NIR transmission spectra measured at $20\text{ }^\circ\text{C}$ and $120\text{ }^\circ\text{C}$ for the three coatings with different thickness are depicted in Fig. 10. They clearly display that the transmission in the infrared (IR) decreases when switching from 20

°C to 120 °C. With increasing coating thickness, the transmission in the visible decreases, and the magnitude of the switch in the IR increases (Fig. 10). For studying the switching kinetics, the transmission at a wavelength of 1600 nm was measured upon increasing the temperature of the module by approximately 1.5 °C·min⁻¹ (Fig. 11a). The transmission at 1600 nm allows the SPT to be monitored as a function of temperature. The transmission as a function of temperature is converted to a conversion-time profile in analogy to the method for powders reported above, and using Lambert-Beer's Law. The conversion is extracted by setting the transmission value around 100 °C to $\alpha = 1$ and the starting transmission (around 20 °C) to $\alpha = 0$ (Fig. 11b). At the conversion of 0.50 the gradient (rate of conversion) is extracted for the different coating thicknesses (Fig. 11c).

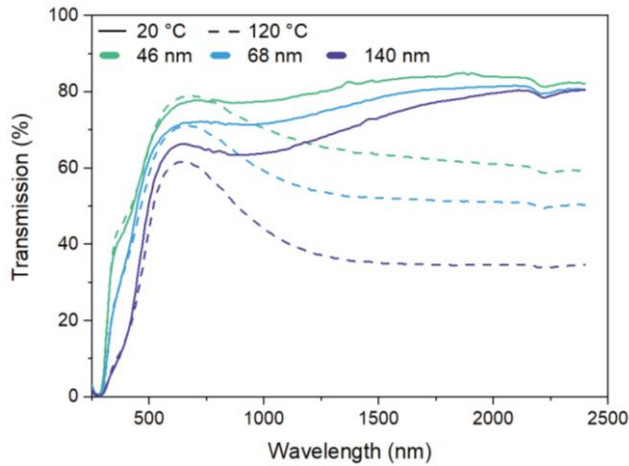


Fig. 10. UV-vis-NIR transmission spectra measured at 20 °C and 120 °C for the various coating thicknesses of 46, 68 and 140 nm.

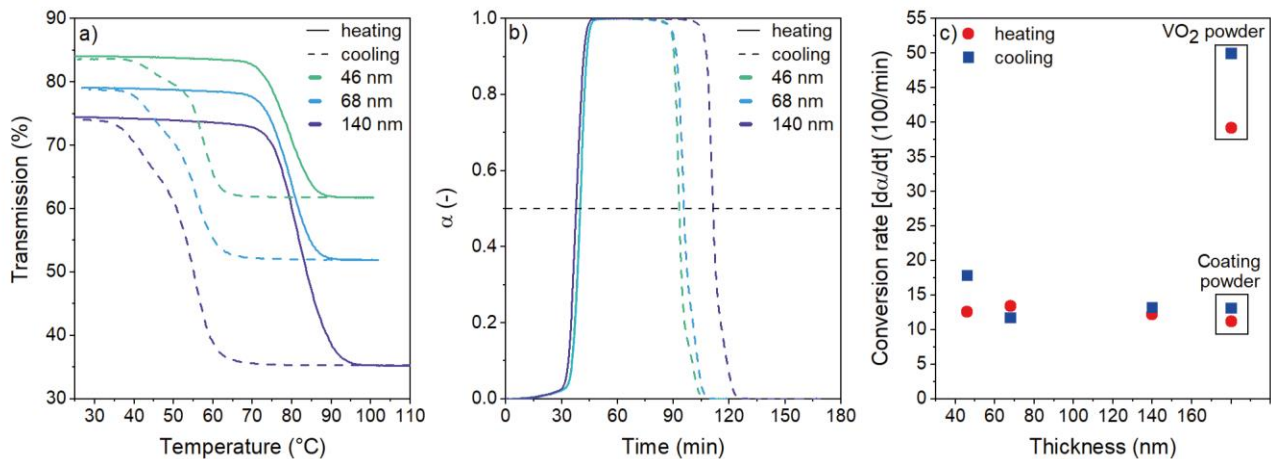


Fig. 11. a) Transmission at $\lambda = 1600$ nm of the VO₂ coatings as function of temperature upon heating and cooling with a rate of 1.5 °C·min⁻¹ for 46, 68 and 140 nm coating thicknesses b) Conversion-time plot for the different coatings for the VO₂ (M) to VO₂ (R) SPT and *vice versa* and c) Conversion rate as function of coating thickness at a heating rate of 1.5 °C·min⁻¹ (coating powder is scraped off coating material).

Due to the thermal lag of the coated glass plate with respect to the temperature imposed by the module, we determined that a heating and cooling rate of 1.5 °C·min⁻¹ was required to accurately monitor the switching kinetics of the coatings. Measurements at higher heating and cooling rates were not feasible, making it impossible to determine the activation barrier of the switch. Nonetheless, we were able to measure the switching rate for the coatings with different thickness at a heating and cooling rate of 1.5 °C·min⁻¹, and compared the rates for three different coating thicknesses (Fig. 11c).

When comparing the rate of the SPT at 50 % conversion for the three different coating thicknesses (Fig. 11c), we observe that the conversion rate is similar for all three coatings, and approximately 4 times lower than for the undoped VO₂ (M) powder. This difference may be caused by the immobilisation of VO₂ (M) on the silica barrier coating and within the silica matrix, making the SPT more difficult to proceed. Furthermore, we observe a small asymmetry for the VO₂ (M) to VO₂ (R) and VO₂ (R) to VO₂ (M) SPT for the 46 nm thick coating, with a slightly higher rate for VO₂ (R) to VO₂ (M). The asymmetry decreases with increasing coating thickness as the rates approach almost

the same values. Additionally, the scraped off material from the 140 nm thick coating, analysed by DSC, and the coating itself display an almost identical switching rate, confirming the quality of the UV-vis-NIR kinetic study.

3.4 Implications for VO₂ application in smart glazing

When applying thermochromic VO₂ particulate materials or coatings for smart glazing applications, the temperature at which the material switches is a key factor determining the energy savings caused by the thermochromic material. [8,17,18] Depending on *e.g.* the type of building, the positioning of the window or facade and the local climate, the ideal switching temperature can vary between 15 °C and 25 °C. Based on our results, we know that the SPT is infinitely slow at the critical switching temperature T_0 , and that a ΔT of 2-3 °C is required to facilitate a fast switch in response to changing environmental conditions. Thus, when a VO₂ (M) to VO₂ (R) switch at 20 °C is required for the specific application, T_0 should be adjusted to 17-18 °C. Furthermore, when lowering the temperature of the glazing unit, a rapid switch of VO₂ (R) to VO₂ (M) is required. In this respect, our powders with ≤ 2 at. % W and our VO₂ coatings outperform the previously reported hydrothermally synthesized particulate materials. [24,25] Latter display an asymmetric behaviour with a significantly slower VO₂ (R) to VO₂ (M) transition. Furthermore, we observed that the purity of VO₂ (M) in the produced powders is much higher than in the coating. *Ergo*, for optimum switching performance it may be worthwhile to produce the high quality powders, reduce their particle size to ≤ 100 nm (*e.g.* by bead milling), and integrate the high-purity VO₂ nanoparticles in a silica matrix to yield optimally performing thermochromic coatings. Based on our results, we may also expect these nanoparticle-based coatings to switch about 4 times faster.

4. Conclusion

We successfully prepared undoped and W-doped VO₂ powders, and undoped VO₂ coatings through solution-phase reduction of V₂O₅ with oxalic acid, and subsequent thermal anneal. Using isoconversional kinetic analysis based on datasets obtained from DSC and UV-vis-NIR spectrophotometry, we studied the rate of the SPT at 50 % conversion of VO₂ (M) powders and coatings, respectively. The high purity undoped VO₂ powder displays a switching temperature ($T_{\alpha=0.02}$) of 66.93 °C and 64.95 °C for the VO₂ (M) to VO₂ (R) and VO₂ (R) to VO₂ (M) SPT, respectively. Doping with W via WCl₆ enabled reducing of the switching temperature to -28.38 °C for the VO₂ (M) to VO₂ (R) SPT. At W concentrations ≤ 2 at. % the SPTs are symmetric, with similar activation energies. The activation energy is temperature dependent, and ranges between 138 and 563 kJ·mol⁻¹ for undoped VO₂ powder. Increasing the difference between the material's temperature and T_0 strongly reduces the activation barrier for the VO₂ (M) to VO₂ (R) and VO₂ (R) to VO₂ (M) SPT. Similar activation energies suggest that similar defects play a key role in both SPTs. However, at higher W concentrations (> 2 at. %) we observed an asymmetric behaviour with a higher activation energy for the switch from VO₂ (R) to VO₂ (M). Undoped VO₂ containing thermochromic coatings applied to SiO₂-coated float glass using a chemical process similar to the one for preparation of powders display a 4 times lower switching rate, which is largely independent from coating thickness. Very thin coatings (46 nm) show asymmetric behaviour with a slightly faster VO₂ (R) to VO₂ (M) transition. This asymmetry is not observed for thicker coatings (68 nm and 140 nm). The results of this study have important implications for application of VO₂ pigments and coatings in thermochromic smart glazing. Pointing out that the switching temperature should be selected 2-3 °C below the desired one to facilitate a rapid switch, and that VO₂ powders with a W concentration ≤ 2 at. % are preferred over hydrothermally synthesized particulate material because of their symmetric switching behaviour. Future studies will focus on the thermochromic properties and thermokinetics of undoped and W-doped VO₂ nanoparticles obtained through bead milling of powders, and nanoparticle based coatings.

Conflicts of interest

There are no conflicts to declare.

Acknowledgements

The authors thank NWO-SIA (RAAK-PRO project Window of the Future) and the European Fund for Regional Development (crossborder collaborative Interreg V program Flanders-the Netherlands, project EnEf) for their financial support. Furthermore, the authors gratefully acknowledge Dr. Marcel Verheijen (Eindhoven University of Technology and Eurofins Materials Science) for the STEM-EDX analysis, Dr. Marta Jezierska-Switala (TNO) for the XRD analysis and Marco Kong for the coating transmission measurements.

References

- [1] M.E.A. Warwick, R. Binions, Advances in thermochromic vanadium dioxide films, *J. Mater. Chem. A*. 2 (2014) 3275–3292. <https://doi.org/10.1039/c3ta14124a>.
- [2] S.-Y. Li, G.A. Niklasson, C.G. Granqvist, Thermochromic fenestration with VO₂-based materials: Three challenges and how they can be met, *Thin Solid Films*. 520 (2012) 3823–3828. <https://doi.org/10.1016/j.tsf.2011.10.053>.
- [3] C.N. Berglund, H.J. Guggenheim, Electronic Properties of VO₂ near the Semiconductor-Metal Transition, *Phys. Rev.* 185 (1969) 1022–1033.
- [4] T. Yao, X. Zhang, Z. Sun, S. Liu, Y. Huang, Y. Xie, C. Wu, X. Yuan, W. Zhang, Z. Wu, G. Pan, F. Hu, L. Wu, Q. Liu, S. Wei, Understanding the nature of the kinetic process in a VO₂ metal-insulator transition, *Phys. Rev. Lett.* 105 (2010) 226405–1–4. <https://doi.org/10.1103/PhysRevLett.105.226405>.
- [5] K. Liu, S. Lee, S. Yang, O. Delaire, J. Wu, Recent progresses on physics and applications of vanadium dioxide, *Mater. Today*. 21 (2018) 875–896. <https://doi.org/10.1016/j.mattod.2018.03.029>.
- [6] M. Li, S. Magdassi, Y. Gao, Y. Long, Hydrothermal Synthesis of VO₂ Polymorphs: Advantages, Challenges and Prospects for the Application of Energy Efficient Smart Windows, *Small J.* 13 (2017). <https://doi.org/10.1002/sml.201701147>.
- [7] S. Ramanathan, ed., *Thin film metal-oxides: Fundamentals and applications in electronics and energy*, Springer, 2010. <https://doi.org/10.1007/978-1-4419-0664-9>.
- [8] D. Mann, C. Yeung, R. Habets, Z. Vroon, P. Buskens, Comparative Building Energy Simulation Study of Static and Thermochromically Adaptive Energy-Efficient Glazing in Various Climate Regions, *Energies*. 13 (2020) 2842.
- [9] N. Peys, P. Adriaenssens, S. Van Doorslaer, S. Gielis, E. Peeters, C. De Dobbelaere, S. De Gendt, A. Hardy, M.K. Van Bael, Aqueous citrate-oxovanadate(IV) precursor solutions for VO₂: synthesis, spectroscopic investigation and thermal analysis, *R. Soc. Chem.* 43 (2014) 12614–12623. <https://doi.org/10.1039/c4dt01346h>.
- [10] G.A. Niklasson, C.G. Granqvist, Electrochromics for smart windows : thin films of tungsten oxide and nickel oxide , and devices based on these, *J. Mater. Chem.* 17 (2007) 127–156. <https://doi.org/10.1039/b612174h>.
- [11] C.G. Granqvist, G.A. Niklasson, Solar energy materials for thermal applications: A primer, *Sol. Energy Mater. Sol. Cells*. 180 (2018) 213–226. <https://doi.org/10.1016/j.solmat.2018.02.004>.
- [12] X. Xiao, H. Zhang, G. Chai, Y. Sun, T. Yang, H. Cheng, L. Chen, L. Miao, G. Xu, A cost-effective process to prepare VO₂ (M) powder and films with superior thermochromic properties, *Mater. Res. Bull.* 51 (2014) 6–12. <https://doi.org/10.1016/j.materresbull.2013.11.051>.
- [13] J. Schläfer, C. Sol, T. Li, D. Malarde, M. Portnoi, T.J. Macdonald, S.K. Laney, M.J. Powell, I. Top, I.P. Parkin, I. Papakonstantinou, Thermochromic VO₂-SiO₂ nanocomposite smart window coatings with narrow phase transition hysteresis and transition gradient width, *Sol. Energy Mater. Sol. Cells*. 200 (2019) 1–7. <https://doi.org/10.1016/j.solmat.2019.109944>.
- [14] D. Wang, D. Guo, Z. Zhao, C. Ling, J. Li, S. Hong, Y. Zhao, H. Jin, Surface modification-assisted solvent annealing to prepare high quality M-phase VO₂ nanocrystals for flexible thermochromic films, *Sol. Energy Mater. Sol. Cells*. 200 (2019) 1–7. <https://doi.org/10.1016/j.solmat.2019.110031>.
- [15] H. Ji, D. Liu, H. Cheng, Y. Tao, Large area infrared thermochromic VO₂ nanoparticle films prepared by inkjet printing technology, *Sol. Energy Mater. Sol. Cells*. 194 (2019) 235–243. <https://doi.org/10.1016/j.solmat.2019.02.028>.
- [16] G. Pan, J. Yin, K. Ji, X. Li, X. Cheng, H. Jin, J. Liu, Synthesis and thermochromic property studies on W doped VO₂ films fabricated by sol-gel method, *Sci. Rep.* 7 (2017) 1–10. <https://doi.org/10.1038/s41598-017-05229-9>.
- [17] M. Saeli, C. Piccirillo, I.P. Parkin, R. Binions, I. Ridley, Energy modelling studies of thermochromic glazing, *Energy Build.* 42 (2010) 1666–1673. <https://doi.org/10.1016/j.enbuild.2010.04.010>.
- [18] R. Tällberg, B.P. Jelle, R. Loonen, T. Gao, M. Hamdy, Comparison of the energy saving potential of adaptive and controllable smart windows: A state-of-the-art review and simulation studies of thermochromic, photochromic and electrochromic technologies, *Sol. Energy Mater. Sol. Cells*. 200 (2019) 1–30. <https://doi.org/10.1016/j.solmat.2019.02.041>.
- [19] W.-K. Hong, S. Cha, J.I. Sohn, J.M. Kim, Metal-Insulator Phase Transition in Quasi-One-Dimensional VO₂ Structures, *J. Nanomater.* 2015 (2015). <https://doi.org/10.1155/2015/538954>.
- [20] Z. Shao, X. Cao, H. Luo, P. Jin, Recent progress in the phase-transition mechanism and modulation of vanadium dioxide materials, *NPG Asia Mater.* 10 (2018) 581–605. <https://doi.org/10.1038/s41427-018-0061-2>.
- [21] Y. Cui, Y. Ke, C. Liu, Z. Chen, N. Wang, L. Zhang, Y. Zhou, S. Wang, Y. Gao, Y. Long, Thermochromic VO₂ for Energy-Efficient Smart Windows, *Joule*. 2 (2018) 1707–1746. <https://doi.org/10.1016/j.joule.2018.06.018>.
- [22] K.L. Gurunatha, S. Sathasivam, J. Li, M. Portnoi, I.P. Parkin, I. Papakonstantinou, Combined Effect of Temperature Induced Strain and Oxygen Vacancy on Metal-Insulator Transition of VO₂ Colloidal Particles, *Adv. Funct. Mater.* 30 (2020) 1–9. <https://doi.org/10.1002/adfm.202005311>.
- [23] S.-Y. Li, G.A. Niklasson, C.G. Granqvist, Thermochromic fenestration with VO₂-based materials: Three challenges and how they can be met, *Thin Solid Films*. 520 (2012) 3823–3828.

- [24] V.A. Blagojević, N. Obradović, N. Cvjetičanin, D.M. Minić, Influence of dimensionality on phase transition in VO₂ nanocrystals, *Sci. Sinter.* 45 (2013) 305–311. <https://doi.org/10.2298/SOS1303305B>.
- [25] H. Zhang, H. Yu, Z. Chen, H. Luo, Y. Gao, Thermal kinetic analysis of metal–insulator transition mechanism in W-doped VO₂, *J. Therm. Anal. Calorim.* 126 (2016) 949–957. <https://doi.org/10.1007/s10973-016-5579-3>.
- [26] S. Vyazovkin, *Isoconversional Kinetics of Thermally Stimulated Processes*, Springer, 2015.
- [27] P. Papon, J. Leblond, P.H.E. Meijer, *The physics of phase transitions: Concepts and applications*, 2nd ed., Springer, 2006. <https://doi.org/10.1007/3-540-33390-8>.
- [28] S. Vyazovkin, N. Sbirrazzuoli, Isoconversional kinetic analysis of thermally stimulated processes in polymers, *Macromol. Rapid Commun.* 27 (2006) 1515–1532. <https://doi.org/10.1002/marc.200600404>.
- [29] H.L. Friedman, New methods for evaluating kinetic parameters from thermal analysis data, *Polym. Lett.* 7 (1969) 41–46.
- [30] G. V. Chandrashekhar, H.L.C. Barros, J.M. Honig, Heat capacity of VO₂ single crystals, *Mater. Res. Bull.* 8 (1973) 369–374. [https://doi.org/10.1016/0025-5408\(73\)90039-1](https://doi.org/10.1016/0025-5408(73)90039-1).
- [31] P. Schilbe, D. Maurer, Lattice dynamics in VO₂ near the metal-insulator transition, *Mater. Sci. Eng.* 370 (2004) 449–452. <https://doi.org/10.1016/j.msea.2003.08.114>.
- [32] Z. Chen, Y. Gao, L. Kang, C. Cao, S. Chen, H. Luo, Fine crystalline VO₂ nanoparticles: Synthesis, abnormal phase transition temperatures and excellent optical properties of a derived VO₂ nanocomposite foil, *J. Mater. Chem. A.* 2 (2014) 2718–2727. <https://doi.org/10.1039/c3ta14612j>.
- [33] C.L. Gomez-Heredia, J.A. Ramirez-Rincon, D. Bhardwaj, P. Rajasekar, I.J. Tadeo, J.L. Cervantes-Lopez, J. Ordonez-Miranda, O. Ares, A.M. Umarji, J. Drevillon, K. Joulain, Y. Ezzahri, J.J. Alvarado-Gil, Measurement of the hysteretic thermal properties of W-doped and undoped nanocrystalline powders of VO₂, *Sci. Rep.* 9 (2019) 1–14. <https://doi.org/10.1038/s41598-019-51162-4>.
- [34] L. Chen, C. Huang, G. Xu, L. Miao, J. Shi, J. Zhou, X. Xiao, Synthesis of thermochromic W-doped VO₂ (M/R) nanopowders by a simple solution-based process, *J. Nanomater.* 2012 (2012) 1–8. <https://doi.org/10.1155/2012/491051>.
- [35] K. Momma, F. Izumi, VESTA 3 for three-dimensional visualization of crystal, volumetric and morphology data, *J. Appl. Crystallogr.* 44 (2011) 1272–1276. <https://doi.org/10.1107/S0021889811038970>.